Earthquake source parameters and scaling relationships at The Geysers geothermal field, California

Vincenzo Convertito (1), Aldo Zollo (2), Nitin Sharma(1,2), Antonella Orefice(2), Antonio Emolo (2)
1. Istituto Nazionale di Geofisica e Vulcanologia, Italy
2. Department of Physics, University of Naples Federico II, Italy

Istituto Nazionale di Geofisica e Vulcanologia

Introduction

Understanding induced seismicity in a geothermal system can help to characterize the geometry, extent and conditions of the reservoir, and to assess the potential seismic hazard associated with field operations. Here we analyze induced seismicity at The Geysers geothermal field in Northern California. The Geysers geothermal field, is a vapor-dominated geothermal field located in Northern California. The main steam reservoir has a temperature of about 235°C and underlies an impermeable caprock with its base at 1.1-3.3 km below the surface. Commercial exploitation of the field began in 1960, and seismicity became more frequent in the area and increased with increasing field development (e.g., Eberhart-Phillips and Oppenheimer, 1984; Majer et al., 2007). Induced seismicity has been monitored since the mid 1970s and its temporal and spatial distributions have been analyzed to understand the causing mechanisms (e.g, Eberhart-Philipps and Oppenheimer, 1984).

The present study reports the results of source parameters' analysis of natural and induced seismicity at The Geysers geothermal field recorded from 2007/07/26 through 2011/10/30, at the dense Lawrence Berkeley National Laboratory Geysers/Calpine (BG) seismic network.

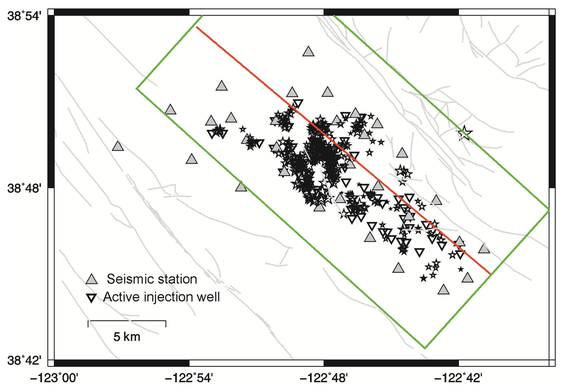

Figure 1: Map of events analyzed in this study. Grey triangles indicate the seismic stations of LBNL seismic network used in this study. Red line identifies the section reported in Figure 2.

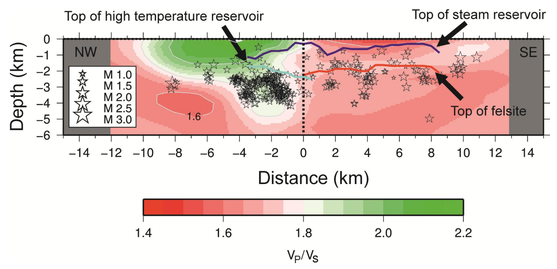

Figure 2: V_P/V_S ratio model along the section indicated in red in Figure 1. The horizon of the reservoirs and of the felsite are redrawn from Beall and Wright (2010).

Method

To determine seismic source parameters we have used a parametric modeling approach, which is combined with a multi-step non-linear inversion strategy that allows to jointly invert source and attenuation parameters, together with site/station correction (Zollo et al., 2014).

Data description

- P- and S-wave displacement spectra of 266 microearthquakes;
- 32 3-component stations managed by Lawrence Berkeley National Laboratory Geysers/Calpine;
- Seismic Moment: $1x10^9$ – $1x10^{15}$ Nm;
- Frequency range: 5.0 - 170 Hz;
- Distance range: 0.2- 27 km;
- Only waveforms with peak-amplitude 3 times larger than noise (pre P);
- Selected time window for P-waves T^P = 2.56s;
- Selected time window for S-waves T^S =3.0 s;

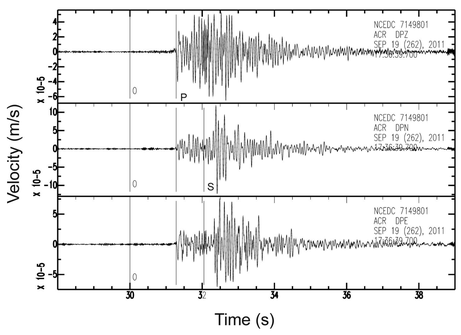

Figure 3: Example of a seismogram relative to a M 1.3 earthquake recorded at R^{epi} =5.9 km.

Spectral model

The recorded P- and S-wave displacement spectra are assumed to be the convolution of four terms

$$U(\omega) = S_0(\omega)\, Q(\omega)\, R(\omega)\, I(\omega)$$

which account for source model, path effects, attenuation effects, site effects and instrumental response. Here we assume that:

○ *Source model*

$$S_0(\omega) = \frac{\Omega_0}{1+\left(\frac{\omega}{\omega_c}\right)^{\gamma}}$$

where Ω_o is the low-frequency spectral level, γ the high-frequency fall-off parameter and ω_c the corner frequency.

○ *Path attenuation*

$$Q(\omega) = e^{-\frac{\omega t^*_c}{2}} \qquad t^* = \frac{T}{Q}$$

where *c* identifies the selected seismic phase and *T* is the travel-time.

○ *Site term*

$$R(\omega) = R^c_j = \frac{1}{M_j}\sum_{j=1}^{M}\frac{\Omega^{ij}_{0c}}{\Omega^{i}_{0c}}$$

where *j* identifies the station and *i* identifies the earthquake.

○ *Overall instrument response I(ω)* contains both sensor and data-logger responses

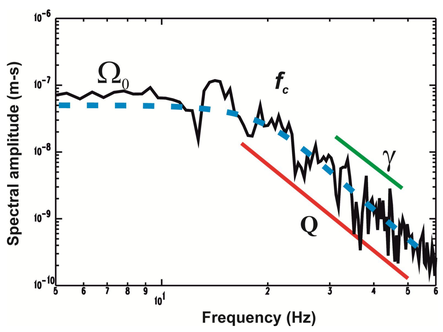

Figure 4: Example of observed and fitted displacement spectrum. The inverted parameters are also indicated.

Iterative, multi-step inversion

The diagram on the right shows the flow of the steps of the iterative multi-step inversion proposed by Zollo et al. (2014). The procedure proved to be able to minimize the dependence between the inverted parameters.

The convergence criteria is based on the observation of no or negligible change in the median value of the *t** and γ estimated from the corresponding distributions.

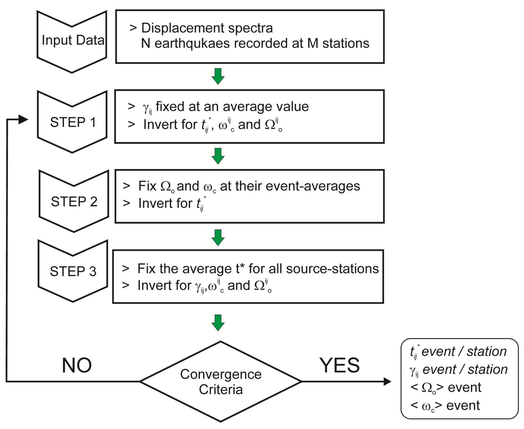

Figure 5

Author contact: vincenzo.convertito@ingv.it

Results

The results of the analysis indicate that a constant Q model can be used to represent the anelastic attenuation in the investigated volume. We found median P and S quality factors equal to Q_P=75 (53,104) and Q_S=65 (44, 96) (the 68.8% confidence intervals are given in parenthesis), which provide a Q_S/Q_P ratio close to unity (median value Q_S/Q_P = 0.9±0.2).

We observe a self-similar scaling of the estimated source parameters in the investigated seismic moment range (Figure 6a), with a nearly constant Madariaga (1976) static stress-drop of 1.7(0.8, 3.8) MPa (Figure 6b). The median values of the P-to-S corner frequencies (fcP/fcS = 1.52) (Figure 6c) is consistent with the dynamic model of an expanding circular crack at a constant stress drop scaling.

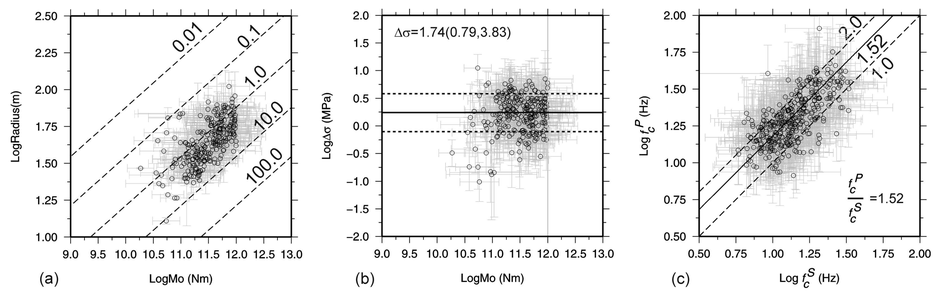

Figure 6: Scaling laws for the analyzed events. The vertical grey line in panel b identifies the upper value that can be estimated due to the instrumental response function.

For the seismic source, we found that the mean value of the high-frequency fall-off parameter *γ* about 2 for both P- and S-wave is consistent with the ω-square source model. A nearly constant apparent stress τ_a of 0.073 (0.027,0.197) MPa, as measured by seismic energy, is observed in the whole analyzed seismic moment range (Figure 7a). The distribution of the Savage-Wood seismic efficiency η_{SW} median value of 0.04 (0.02, 0.1) indicates a rather small radiation efficiency (Figure 7b) suggesting that a large positive dynamic overshoot could be the dominant mechanism the micro-earthquake fractures in the volume investigated in the present study.

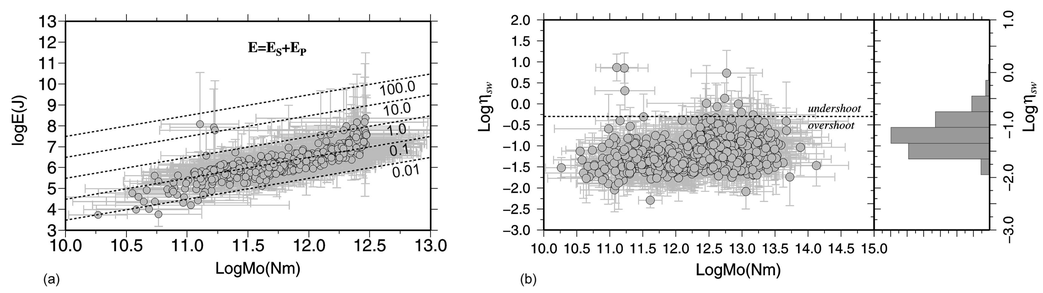

Figure 7: Panel a: Total radiated energy versus seismic moment. Dashed lines refer to constant apparent stress values expressed in MPa. Panel b : The Savage-Wood seismic efficiency versus seismic moment and histogram of the observed values. The dashed line corresponds to the threshold 0.5, limiting the undershoot from overshoot dynamic weakening mechanisms.

Several studies indicate that The Geysers is characterized by differences in temperature, seismicity rate and depth of the events moving from NW to SE (Beall and Wright, 2010; Convertito et al., 2012). In accordance with previous observations, seismic tomography results obtained by Amoroso et al.(2015), show a variation in the mechanical properties (V_P, V_S and V_P/V_S) of the rocks along the same direction. In particular, the area at NW characterized by a relatively high V_P/V_S ratio (at depths 2.5-5.0km) (Figure 2), has temperatures as high as 360° (Beall and Wright, 2010).

We investigate how source parameters vary with depth and if they differ for the two areas (Figure 2). The results reported in Figure 8 show that static stress-drop slightly increases with depth and that the events occurring in the two areas are characterized by slightly different seismic energy, efficiency and corner frequencies.

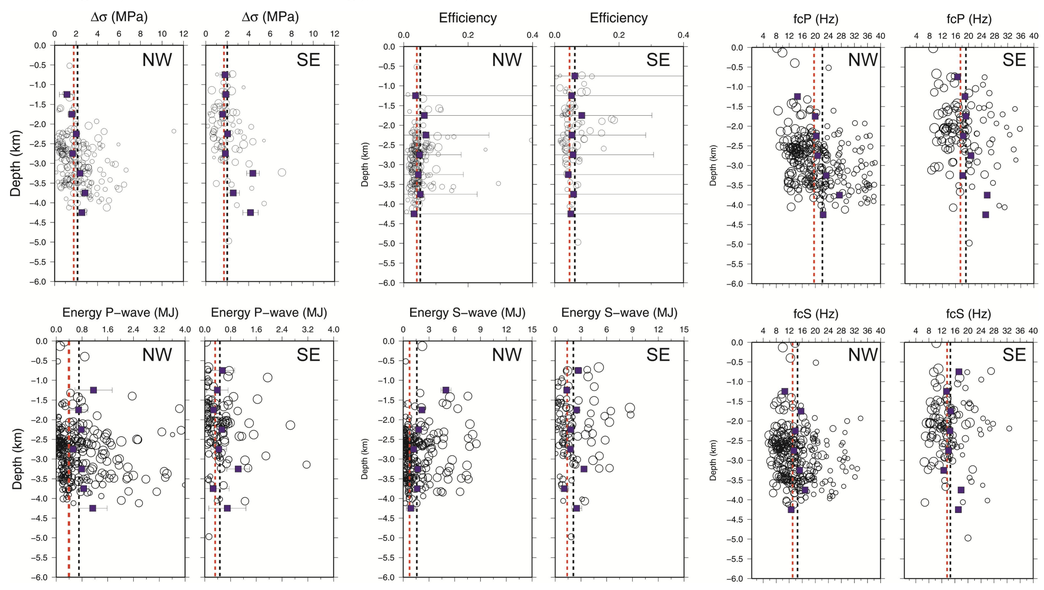

Figure 8: Source parameters, seismic energy and efficiency as function of depth. Red line indicates the median value while black line the mean value.

Conclusions

- The found self-similar, constant stress-drop source parameter scaling and the observed fcP/fcS(=1.52) corner frequency ratio suggest that microearthquake ruptures at The Geysers are well reproduced by the Madariaga(1976) circular shear crack model expanding at an uniform rupture velocity.
- We found low-values of Savage-Wood seismic efficiency (η_{SW}~0.04), with positive overshoot. This value is consistent with the theoretical estimate obtained by Singh and Ordaz (1994) assuming an ω-square spectral model to estimate the seismic energy and the Madariaga rupture model to infer the rupture radius from the corner frequency.
- We found low static stress-drop values $\Delta\sigma$~1.7(0.8, 3.8) MPa. This value is consistent with the average stress drop value shown by Tomic et al. (2009) for induced earthquakes. We ascribe this conclusion to a low yelding stress level, due to the repeated rupture of pre-fractured rocks.
- Since the events mainly occur in the volume of high temperature, where also a relatively high V_P/V_S ratio has been observed, we interpret the analyzed seismic events as thermally induced microcracks. The thermal contrast being due to the injection of cold water in dry hot rocks.

References

• Amoroso, O. , G. De Landro , G. Russo and A. Zollo (2015). 4D imaging of elastic/anelastic medium properties: application to the Geyser geothermal area. This workshop.
• Beall, J. J. and M. C. Wright (2010). Southern Extent of The Geysers High Temperature reservoir based on seismic and geochemical evidence, Geothermal Resources Council Transactions, 34, 53-56.
• Convertito V., N. Maercklin, N. Sharma, and A. Zollo (2012). From Induced Seismicity to Direct Time-Dependent Seismic Hazard, Bull. Seismic. Soc. Am., 102, 6, pp. 2563–2573, DOI: 10.1785/0120120036.
• Eberhart-Phillips, D., and D. H. Oppenheimer (1984). Induced seismicity in The Geysers Geothermal Area, California. J. Geophys. Res., 89, 1191–1207.
• Madariaga, R., (1976). Dynamics of an expanding circular fault, Bull. Seismol. Soc. Am., 66, 639-666.
• Majer, E.L., and J. E. Peterson (2007). The impact of injection on seismicity at The Geysers, California Geothermal Field. Int. J. Rock Mech. Mining.
• Singh, S. K., and M. Ordaz (1994). Seismic energy release in Mexican subduction zone earthquakes,Bull. Seism. Soc. Am. 84, 1533–1550.
• Tomic, J., R. E. Abercrombie, and A. do Nascimento (2009). Source parameters and rupture velocity of small M≤2.2 reservoir induced earthquakes, Geophys. J. Int., doi:10.1111/j.1365-246X.2009.04233.x
• Zollo, A., A. Orefice, and V. Convertito (2014). Source Parameter Scaling and Radiation Efficiency of Microearthquakes Along the Irpinia Fault Zone in Southern Apennines, Italy, J. Geophys. Res., 119, 4, 3256–3275. DOI: 10.1002/2013JB010116.